Journal of Theoretical and Applied Physics (JTAP), Vol.16, No. 4, 162242 (1-8), 2022
Received 5 July 2022 ; Accepted 9 October 2022 ; [http://dx.doi.org/10.30495/jtap.162242]

The influence of Hively and Bosch-Hale reactivities on hot ion mode in deuterium/helium-3 fuel

Armin Taghipour[1], S. Mohammad Motevalli[1]*, Fereshteh Fadaei [2]

Abstract
Nowadays, there is much extensive research investigating nuclear fusion reaction with D-^{3}He fuel as one of the most essential advanced fusion fuels. One of the most important quantities in fusion is the reactivity. In this work, with consideration of different temperatures for ion and electron (hot ion mode), we intend to study the effects of two different reactivities (Hively and Bosch-Hale) on D-^{3}He fusion reaction in spherical tokamak. Accordingly, by writing the system of particle and energy balance equations for this reaction in hot ion mode, we will investigate the effects of reactivities on plasma parameters in spherical tokamak.

Keywords
D-^{3}He fusion, Spherical tokamak, Particle and energy equation, Reactivity.

[1] *Department of Physics, Faculty of Science, University of Mazandaran, Babolsar, Iran.*
[2] *Department of Physics, Payam Noor University, Tehran, Iran.*
***Corresponding author**: motavali@umz.ac.ir*

1. Introduction

One way to achieve nuclear fusion is to confine the plasma by using a magnetic field. Up to now, the tokamak system is recognized as one of the most successful magnetic confinement fusion devices [1]. In this system, the effect of the magnetic field on charged particles is used to confine the hot plasma. Most of the experiments performed in the field of nuclear fusion were on D-T fuel, which, one of the most important reasons for this matter is to perform this reaction at a lower temperature (compared to other fusion reactions) and having the highest reactivity in the intended temperature range in fusion reactors. However, disadvantages include high radiation, the possibility of a meltdown in the reactor, and the lack of natural resources of tritium (which, to solve this problem, lithium blankets are used to produce tritium in the reactor), have attracted attention to other fuels. In the meantime, D-^{3}He fuel has been considered by a large number of researchers because of its advantages such as direct energy conversion and fewer dangers due to radiation, the impossibility of meltdown, higher efficiency, and lower cost (more straightforward structure due to no need to use blankets) [2–10]. Another noteworthy point about D-^{3}He fuel is the issue of tokamak structure. High aspect ratio tokamak reactors are unsuitable for D-^{3}He fusion operation due to their high toroidal magnetic field and low beta. After investigating the ignition capabilities of two models of spherical tokamak reactors and high aspect ratio tokamaks for D-^{3}He fuel, the researchers found that in a spherical tokamak, the power fraction required for ions in the hot ion mode ($T_i > T_e$) is smaller due to lower synchrotron radiation loss. Therefore, spherical tokamak has been considered due to its low aspect ratio [11–18]. In spherical tokamaks, unlike conventional tokamaks, with a generally round donut-like confinement area with large cavities in the middle, the size of the cavities is reduced as much as possible, resulting in an almost spherical plasma shape [19–25]. On the other hand, a significant quantity to consider in the study of fusion fuels is reactivity (the $\langle\sigma v\rangle$ parameter). This quantity is defined as the probability of reacting per time unit per the target nuclear density unit, and it is a function of plasma temperature (in units of keV) which in the simplest case is specified only by the $\langle\sigma v\rangle$ parameter. The $\langle\sigma v\rangle$ parameter is often referred to as the reactivity parameter [26–30].

2. Fusion power and reactivity

If only one type of fusion process occurs at the rate of density Rfu with the unit of released energy on the Q_{fu} reaction, then the fusion power produced per volume unit is given by the following equation

$$P_{fu} = \propto R_{fu} Q_{fu} \tag{1}$$

If the unit of R_{fu} is based on $m^{-3}s_{-1}$ and the Q_{fu} unit is based on MeV for each reaction, the unit of fusion density P_{fu} will be $MeVm^{-3}s_{-1}$ and the total energy released for a uniform distribution of power over the time interval τ and volume V is thus

$$E^*_{fu} = V \int_0^{\tau} P_{fu} dt \tag{2}$$

and for each time t

$$P_{fu} = \left(\frac{dE^*_{fu}}{dt}\right)\frac{1}{V} \tag{3}$$

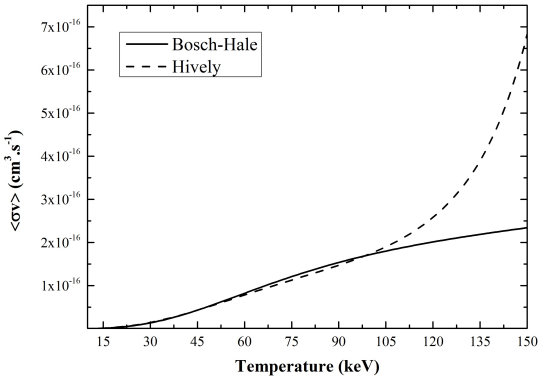

Figure 1. The D-^{3}He fusion reactivity as a function of temperature.

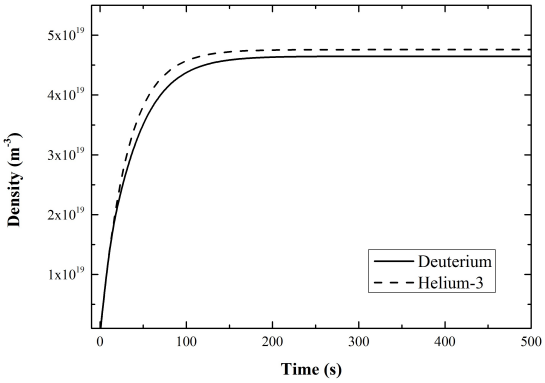

Figure 2. The temporal evolution of deuterium and helium-3 particle densities based on Hively reactivity.

The energy produced in a fusion reaction, Q_{fu}, is called the "Q value" of the reaction, and can be obtained experimentally or through existing tables. To determine the expression for the fusion reactivity density, we consider two particles, a and b, the number densities of them are N_a and N_b, respectively. If v_r is the relative velocity of the two particles at the intersection point and consider the cross-section as $\sigma_{ab}(v_r)$, the explicit equation of the fusion reactivity density will be as follows [31]

$$R_{fu} = \sigma_{ab}(v_r) N_a N_b v_r \tag{4}$$

3. Reactivity of nuclear fusion reactions ($\langle\sigma v\rangle$ Parameter)

A vital quantity to consider in the study of fusion fuels is the reactivity. This quantity is defined as the probability of reacting per time unit on the target nuclear density unit, and it is a function of plasma temperature (in units of keV). This quantity is specified by the $\langle\sigma v\rangle$ parameter. This parameter is called the "Sigma-Vi" parameter (reactivity parameter). In general, with consideration of the relative velocity v for each pair of nuclei that collide, the motion of the target nucleus is different. In this case, we will get an average value, which is specified in the following equation.

$$\langle\sigma v\rangle = \int_0^\infty \sigma(v) v f(v) dv \tag{5}$$

In equation (5), $f(v)$ is a scattering function related to relative velocities, which are normalized as $\int_0^\infty f(v)dv$. The effectiveness of the fusion fuel is determined by its reactivity ($\langle\sigma v\rangle$) [32].

4. $\langle\sigma v\rangle$ Parameter calculations

The Maxwell velocity scattering equation is specified by the following statement

$$f_i(v_i) = \left(\frac{m_j}{2\pi k_B T}\right)^{\frac{3}{2}} e^{-\frac{m_j v_j^2}{2k_B T}} \tag{6}$$

index j identifies the species. T illustrates temperature, and k_B illustrates the Boltzmann constant. The expression for the average reactivity can be rewritten in the form of the following equation

$$\langle\sigma v\rangle = \int\int dv_1 dv_2 \sigma_{1,2}(v) v f_1(v_1) \tag{7}$$

which $v = |v_1 - v_2|$ and integrals are calculated on the three-dimensional velocity space. In equation (7), to get a suitable form to integrate, the velocities v_1 and v_2 are written by the center of mass relative velocities. Therefore, we will have

$$\langle\sigma v\rangle = \frac{(m_1 m_2)^{\frac{3}{2}}}{(2\pi k_B T)^3} \int\int dv_1 dv_2 e^{-\frac{(m_1+m_2)v_c^2}{2k_B T} - \frac{m_r v^2}{2k_B T}} \sigma(v) v \tag{8}$$

which $m_r = (m_1 m_2)/(m_1 + m_2)$ and indicates that integration over $dv_1 dv_2$ can be replaced by integration over $dv_c dv$. If we write the volumetric element in velocity space as $dV = 4\pi v^2 dv$, by using the definition of the energy of the center of mass as $\varepsilon = 1/2 m_r v^2$, we will finally reach the following equation.

$$\langle\sigma v\rangle = \frac{4\pi}{(2\pi m_r)^{\frac{1}{2}}} \frac{1}{(k_B T)^{\frac{3}{2}}} \int_0^\infty \sigma(\varepsilon) \varepsilon e^{-\frac{\varepsilon}{k_B T}} d\varepsilon \tag{9}$$

The fusion cross-section equation for all fusion reactions is shown in the following equation [33].

$$\sigma(E_{lab}) = -16389 C_3 \left(1 + \frac{m_a}{m_b}\right)^2 \times [m_a E_{lab} [e^{(31.40 Z_1 Z_2 \sqrt{\frac{m_a}{E_{lab}}})} - 1]$$

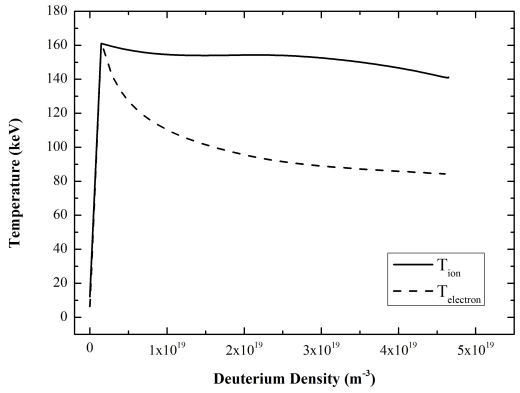

Figure 3. The ion and electron temperatures as a function of deuterium density changes based on Hively reactivity for 500 seconds.

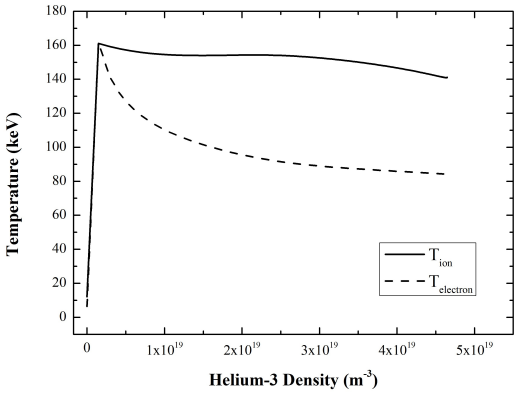

Figure 4. The ion and electron temperatures as a function of helium-3 density changes based on Hively reactivity for 500 seconds.

$$\times\{(C_1+C_2E_{lab})^2+(C_3-\frac{2\pi}{e^{31.40Z_1Z_2\sqrt{\frac{m_a}{E_{lab}}-1}}})^2\}]^{-1} \quad (10)$$

The values of C_1, C_2, and C_3 are determined by the type of reaction [33]. Also m_a and m_b are the mass number of the striking nucleus and the target nucleus, respectively (for example, for deuterium as the colliding nucleus, there is m_a=2). E_{lab} (fuel energy in the laboratory system) is in keV unit, and σ is in barn unit [32–35].

5. Effects of different $\langle\sigma v\rangle$ on plasma parameters

In the previous section, we briefly explained how to calculate the $\langle\sigma v\rangle$ parameter based on the Maxwell distribution. Now, by using the equations calculated for the $\langle\sigma v\rangle$ parameter by Hively and Bosch-Hale, we write the system of particle and energy balance equations for the D-^{3}He reaction. It should be noted that due to the high temperature required for the D-^{3}He fusion reaction, there is a possibility of D-T reaction and two D-D reaction channels. Accordingly, we rewrite the particle and energy balance equations considering four fusion reactions (D-^{3}He, two channels of D-D, and D-T) [10, 36]. Before expressing the system of particle and energy balance equations, we will introduce the equations used for the $\langle\sigma v\rangle$ parameter. The temperature-dependent equation of Hively reactivity is expressed as follows.

$$\langle\sigma v\rangle = e^{\frac{a_1}{T^r}+a_2+\frac{a_3}{T}+\frac{a_4}{T^2}+\frac{a_5}{T^3}+\frac{a_6}{T^4}} \quad (11)$$

The values of a_i and r for D-^{3}He reaction and other reactions are given in the tables in the reference [37].

The Bosch-Hale reactivity equation is also temperature-dependent and is shown by the following equation.

$$\langle\sigma v\rangle = C_1\theta\sqrt{\frac{\zeta}{m_rC^2T^3}}e^{-3\zeta} \quad (12)$$

$$\zeta = (\frac{B_G^2}{4\theta})^{\frac{1}{3}} \quad (13)$$

$$\theta = \frac{T}{1-\frac{T(C_2+T(C_4+TC_6))}{1+T(C_3+T(C_5+TC_7))}} \quad (14)$$

Numerical values of the constants C_1 to C_7 and also the values of m_rc^2 (keV) and $B_G(\sqrt{keV})$ for the D-^{3}He fusion reaction and other side reactions are given in the tables in reference [34].

Now we rewrite the system of particle and energy balance equations considering the four reactions mentioned, and then, for each one of the mentioned $\langle\sigma v\rangle$ equations (eq. 11 and eq. 12), we solve these equations numerically separately and examine the results. It is important to note that this set of equations is written in zero-dimensional model [38–40].

The system of equations includes the differential equations of the change rate of the density of deuterium, helium-3, tritium, proton, and alpha particles relative to time and the temperature changes of ions and electrons concerning the hot ion mode relative to time [38-40]. Generally, for the particles balance equations we have

$$\frac{dn_k}{dt} = -\frac{n_k}{\tau_p^k}+S_k+\sum_{i,j}n_in_j\delta_{ij}\langle\sigma v\rangle_{ij}-\sum_i n_in_k\langle\sigma v\rangle_{ik} \quad (15)$$

where i and j represent suitable species for $i+j\rightarrow k$ reaction. The term of $\frac{n_k}{\tau_p^k}$ is the diffusion loss term and S_k is the external particle supply of the k nucleus. $\langle\sigma v\rangle_{ij}$ is the fusion reactivity for all production and consumption particles (i,j,k = D,^{3}He, T, p, α). The particle balance equations are mentioned in detail in reference [14].

As well as, for the ion temperature equilibrium equation, we

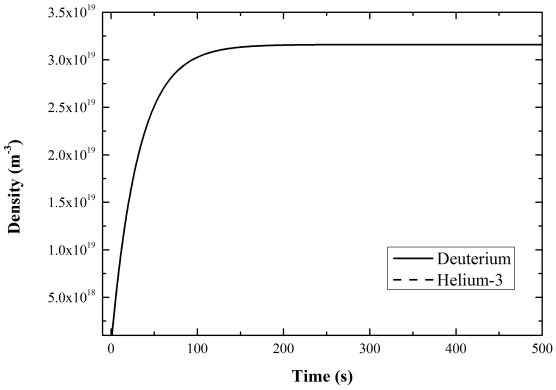

Figure 5. The temporal evolution of deuterium and helium-3 particle densities based on Bosch-Hale reactivity.

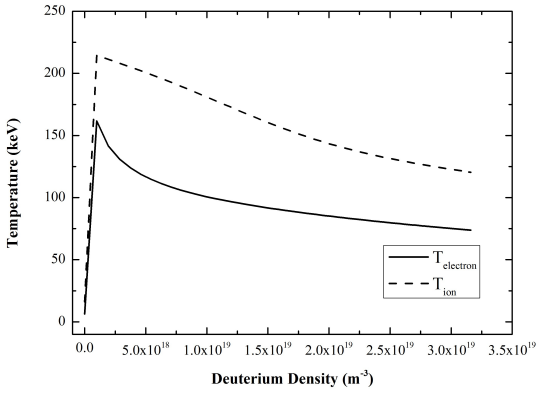

Figure 6. The ion and electron temperatures as a function of deuterium density changes based on Bosch-Hale reactivity for 500 seconds.

have

$$\frac{dT_i(t)}{dt} = \frac{\frac{2}{3}(1+\alpha_n+\alpha_T)}{(\sum_j f_j(t))n_e(t)}[P_{fu}+\frac{P_{EXT}}{V_0}-P_{ie}-P_{Li}]-$$

$$\frac{T_i(t)}{(\sum_j f_j(t))n_e(t)}(\frac{dn_i(t)}{dt}) \quad (16)$$

and for the electron temperature equilibrium equation.

$$\frac{dT_e(t)}{dt} = \frac{\frac{2}{3}(1+\alpha_n+\alpha_T)}{(n_e(t)}[P_{fu}+\frac{P_{EXT}}{V_0}+P_{oh}+P_{ie}-$$

$$P_s-P_b-P_{Le}]-\frac{T_e(t)}{n_e(t)}(\frac{dn_e(t)}{dt}) \quad (17)$$

In equations (16) and (17), $f_j(t)=\frac{n_j(t)}{n_e(t)}$ and the j index represent the D,^{3}He, p, α, and T particles. $n_i(t)$ and $n_e(t)$ represent the ion and the electron density, V_0 is the plasma volume α_n and α_T are the density and temperature profiles, P_{fu}, P_{EXT}, P_{oh}, P_b, P_s, P_{ie} are the fusion product heating power density, the external heating power, the ohmic heating power density, the bremsstrahlung loss power density for electron-electron interactions, the synchrotron radiation loss power density, the density of transferred power by collisions due to the ion and electron temperature difference, respectively. Also, P_{Le} and P_{Li} are the electron and ion conduction loss, respectively. All used parameters in equations (16) and (17), are described in detail in reference [14, 41–44].

The bremsstrahlung loss power (P_b) and synchrotron radiation loss (P_s), with consideration of the relativistic effects, are expressed as follows.

$$P_b = A_b n_e^2(t) \quad (18)$$

$$A_b 1.5\times10^{-38}Z_{eff}[\frac{1}{1+2\alpha_n+0.5\alpha_T}+\frac{1}{1+2\alpha_n+1.5\alpha_T}\times$$

$$\frac{2T_e(t)}{mc^2}]\sqrt{T_e(t)}+3.0\times10^{-38}[\frac{1}{1+2\alpha_n+1.5\alpha_T}+\frac{0.5}{1+2\alpha_n+2.5\alpha_T}$$

$$\{\frac{T_e(t)}{mc^2}\}-\frac{3}{1+2\alpha_n+3.5\alpha_T}\{\frac{T_e(t)}{mc^2}\}^2]\frac{2T_e^{1.5}(t)}{mc^2} \quad (19)$$

$$P_s = A_s n_e^2(t) \quad (20)$$

$$A_s = 2.5\times10^{-56}T_e^4(t)(\frac{T_i(t)}{T_e(t)})^{1.5}\frac{[(\sum_j f_j)+(\frac{T_e(t)}{T_i(t)})]^{1.5}}{\beta(t)^{1.5}\sqrt{aB_{to}}}$$

$$\{f_H+(1-f_H)\sqrt{1-R_{eff}}\}\times\int_0^1[(1-x^2)^{0.5\alpha_n+2.5\alpha_T}$$

$$\{1+\frac{T_e(t)(1-x^2)^{\alpha_T}}{204}\}\times\{1-\beta(t)(1-x^2)^{\alpha_n+\alpha_T}\}^{\frac{5}{4}}$$

$$\sqrt{\sqrt{T_e(t)}(1-x^2)^{0.5\alpha_T}+\frac{2a}{R_0}\sqrt{\frac{mc^2}{2\pi}}}]2xdx \quad (21)$$

R_{eff} is the wall reflectivity, f_H is the hole fraction for divertor and ports (f_H=0.1), $Z_{eff}=\sum_j Z_j^2 n_j/n_e$ is the effective charge, and, $\beta(t)$ is the central toroidal beta that is given by [45, 46]

$$\beta(t) = \langle\beta\rangle(1+\alpha_n+\alpha_T) \quad (22)$$

where $\langle\beta\rangle$ is the average toroidal beta[14].

Now, by using the system of particle balance equations and equations (16) and (17), we can rewrite the particle and energy

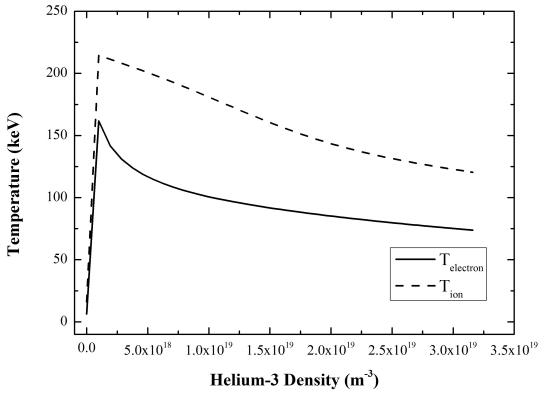

Figure 7. The ion and electron temperatures as a function of helium-3 density changes based on Bosch-Hale reactivity for 500 seconds.

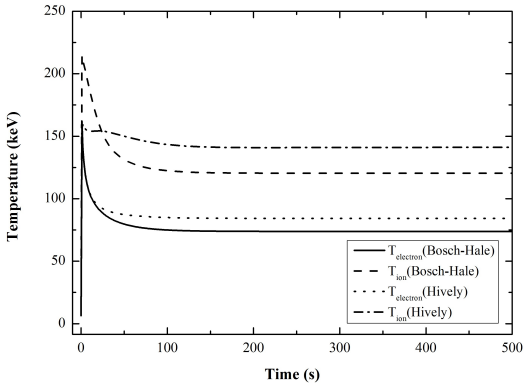

Figure 9. The temporal evolution of ion and electron temperatures based on Hively and Bosch-Hale reactivities.

balance equations, taking into account the hot ion mode, as a system of differential equations of temporal evolution of particles density and ion and electron temperatures, and then, by numerically solving this system for two different $\langle \sigma v \rangle$ (Hively and Bosch-Hale), we examine the results.

In figure 1, Hively and Bosch-Hale reactivities have been demonstrated as a function of temperature in the range of 0 to 200 keV. At first, we will examine the results obtained for the system of particle and energy balance equations based on the Hively $\langle \sigma v \rangle$ equation.

Figure 2 shows that after $\sim$100 seconds, the densities of deuterium and helium-3 particles will achieve steady state. In the following, we will study the ion and electron temperatures as a function of the density of the reaction fuel, i.e., deuterium and helium-3 particles. Figures 3 and 4 show the ion and electron temperature as a function of deuterium and helium-3 particle density changes, respectively. These diagrams are also drawn taking into account the hot ion mode.

What can be seen in figures 3 and 4 is that by increasing particle density, ion and electron temperatures decrease due to loss powers. Another noteworthy point is that the electron temperature in both diagrams has decreased more than the ion temperature, which indicates the effects of the bremsstrahlung loss power and synchrotron radiation loss which can also be seen in the written equations for ion and electron temperatures (equations 16 and 17).

secondly, we examine the results obtained for the system of particle and energy balance equations based on the Bosch-Hale $\langle \sigma v \rangle$ equation. Figure 5 shows the temporal evolution of the densities of deuterium and helium-3 particles for 500 seconds.

The exciting point about figure 5 is that when we use the Bosch-Hale reactivity for the particle and energy balance equation, the graphs of the deuterium and helium-3 particle density variations fit precisely together. It is also observed that

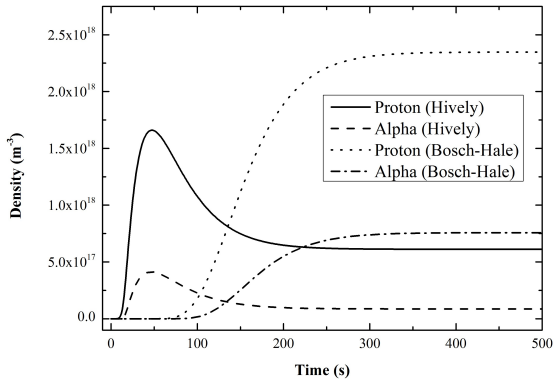

Figure 8. The temporal evolution of proton and alpha particle densities (fusion reaction products) for both Hively and Bosch-Hale reactivities.

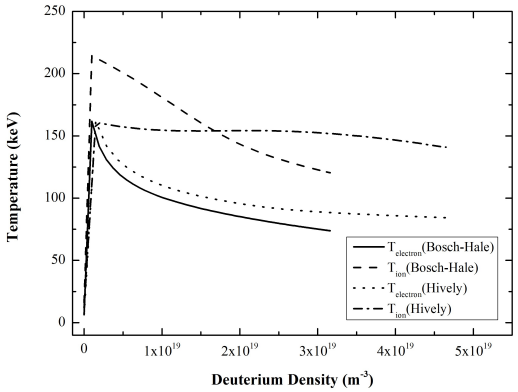

Figure 10. The ion and electron temperatures as a function of deuterium density changes based on Hively and Bosch-Hale reactivities for 500 seconds.

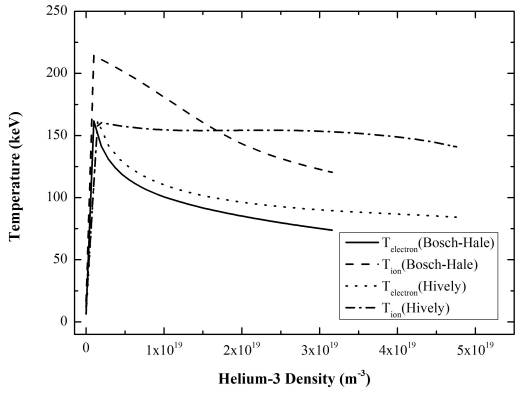

Figure 11. The ion and electron temperatures as a function of helium-3 density changes based on Hively and Bosch-Hale reactivities for 500 seconds.

after ∼100 seconds, the densities of deuterium and helium-3 particles achieve steady state.

In the following, we will examine the ion and electron temperatures as a function of the density of the reaction fuel, i.e., deuterium and helium-3 particles variations. However, this time we use the Bosch-Hale reactivity. Figures 6 and 7 show the ion and electron temperatures as a function of deuterium and helium-3 particle densities variations, respectively. Figures 6 and 7 show that with increasing particle density, ion and electron temperatures decrease due to loss powers. We also see a further decrease in the temperature of the electrons in both figures 6 and 7, which shows the effects of the bremsstrahlung loss power and synchrotron radiation loss (equations 16 and 17).

Now we want to investigate the hot ion mode for both Hively and Bosch-Hale reactivities by comparing the graphs obtained for the ion and electron temperatures as a function of time and the densities of deuterium and helium-3 particles. First, we study the temporal evolution of fusion product densities (proton and alpha particles) for two different reactivities of Hively and Bosch-Hale. Figure 8 shows the temporal evolution of proton and alpha particle densities for both the Hively and Bosch-Hale reactivities.

Figure 8 shows that the densities of the D-^{3}He fusion reaction products (proton and alpha particles) will reach steady state after ∼200 seconds. We should note that the proton and alpha particle densities are more significant when using the Bosch-Hale reactivity than when using the Hively reactivity. Then in figure 9, we see the temporal evolution of ion and electron temperatures for two different reactivities (Hively and Bosch-Hale).

Here we introduce a parameter called the δ parameter as an indicator of the temperature ratio of ions to electrons. After ∼100 seconds, when the ion and electron temperatures reach steady state for both reactivities, we compute the δ parameter for two different Hively and Bosch-Hale reactivities:

$$\delta_{(Hively)} = \frac{T_{i(Hively)}}{T_{e(Hively)}} \cong 1.68$$

$$\delta_{(Bosch-Hale)} = \frac{T_{i(Bosch-Hale)}}{T_{e(Bosch-Hale)}} \cong 1.63$$

Figure 9 shows that the temperatures obtained for ions and electrons using the Hively reactivity, when achieved to steady state, are higher than those obtained for ions and electrons achieved by using the Bosch-Hale reactivity. However, the ion to electron temperature ratio (δ parameter) is almost the same value for both reactivities. In the following, figures 10 and 11 show the ion and electron temperature as a function of deuterium and helium-3 densities changes for both Hively and Bosch-Hale reactivities, respectively.

6. Conclusion

With consideration of hot ion mode, we intend to investigate the effects of Hively and Bosch-Hale reactivities on D-^{3}He fusion reaction in spherical tokamak. Then, by writing the system of particle and energy balance equations for this reaction, we studied the effects of two different reactivities on plasma parameters in spherical tokamak. Eventually, we saw that the value of the δ parameter is almost the same for both reactivities (Hively and Bosch-Hale). In other words, for both Hively and Bosch-Hale reactivities, in the hot ion mode, the ion to electron temperature ratio will not change so much. Also, in figures 10 and 11, it can be seen that ion and electron temperatures as a function of density based on the Bosch-Hale reactivity have a steeper decreasing gradient than the Hively reactivity. Another critical point is that when we used the Hively reactivity to calculate the system of particle and energy balance equations, ion and electron temperatures compared to variations in fusion fuel density of D-^{3}He (deuterium and helium-3 particles) had more stability than using the Bosch-Hale reactivity to calculate the particle and energy balance equations.

Conflict of interest statement:

The authors declare that they have no conflict of interest.

References

[1] J. Citrin, J. Garcia, T. G¨orler, F. Jenko, P. Mantica, D. Told, C. Bourdelle, D. R. Hatch, G. M. D. Hogeweij, T. Johnson, M. J. Pueschel, M. Schneider, and JET-EFDA Contributors. *Plasma Physics and Controlled Fusion*, **57**:014032, 2014.

[2] B. Coppi. *Physica Scripta*, **1982**:590, 1982.

[3] L. El-Guebaly and M. Zucchetti. *Fusion engineering and design*, **82**:351, 2007.

[4] J. D. Galambos and Y. K. M. Peng. *Fusion Technology*, **19**:31, 1991.

[5] N. Holtkamp. *Fusion Engineering and Design*, **84**:98, 2009.

[6] G. L. Kulcinski, J. P. Blanchard, G. A. Emmert, L. A. El-Guebaly, H. Khater, C. W. Maynard, E. A. Mogahed, J. E Santarius, M. E. Sawan, and I. N. Sviatoslavsky L. J. Wittenberg. *Fusion Technology*, **21**:1779, 1992.

[7] P. Rodriguez-Fernandez, N. T. Howard, M. J. Greenwald, A. J. Creely, J. W. Hughes, J. C. Wright, C. Holland, Y. Lin, and F. Sciortino and. *Journal of Plasma Physics*, **86**:1, 2020.

[8] J. Santarius, G. Kulcinski, and L. El-Guebaly. *Fusion science and technology*, **44**:289, 2003.

[9] S. M. Motevalli and F. Fadaei. *Zeitschrift für Naturforschung A*, **70**:79, 2015.

[10] S. Motevalli and F. Fadaei. *Pramana*, **86**:837, 2016.

[11] S. M. Kaye, M. G. Bell, R. E. Bell, S. Bernabei, J. Bialek, T. Biewer, W. Blanchard, J. Boedo, C. Bush, M. D. Carter, W. Choe, N. Crocker, D. S. Darrow, W. Davis, L. Delgado-Aparicio, and et al. *Nuclear fusion*, **45**:S168, 2005.

[12] E. J. Lerner. *Prospects for p11B fusion with the dense plasma focus: new results*. Current Trends in International Fusion Research, 5th edition, 2008.

[13] C. Liao, B. Labombard, B. Lane, and M. S. Kazimi. *Fusion technology*, **21**:41, 1992.

[14] O. Mitarai. *Nuclear Reactors, Nuclear Fusion and Fusion Engineering*, :405, 2009.

[15] O. Mitarai, H. Matsuura, and Y. Tomita. *Fusion engineering and design*, **81**:2719, 2006.

[16] O. Mitarai, A. Sagara, S. Imagawa, Y. Tomita, K. Watanabe, and T. Watanabe. *Journal of Plasma and Fusion Research Series*, **6**:303, 2004.

[17] F. Najmabadi, R. W. Conn, C. G. Bathke, J. P. Blanchard, L. Bromberg, J. Brooks, E. T. Cheng, D. R. Cohn, D. A. Ehst, L. A. El-Guebaly, G. A. Emmert, T. J. Dolan, and et al. *The 14th IEEE/NPSS Symposium Fusion Engineering*, **1**:213, 1991.

[18] S. Shiraiwa, S. Ide, S. Itoh, O. Mitarai, O. Naito, T. Ozeki, Y. Sakamoto, T. Suzuki, Y. Takase, S. Tanaka, T. Taniguchi, M. Aramasu, T. Fujita, T. Fukuda, X. Gao, M. Gryaznevich, K. Hanada, E. Jotaki, Y. Kamada, T. Maekawaa, Y. Miuraa, K. Nakamura, T. Nishi, H. Tanaka, and K. Ushigusa. *Physical review letters*, **92**:035001, 2004.

[19] G. Federici, C. H. Skinner, J. N. Brooks, J. P. Coad, C. Grisolia, A. A. Haasz, A. Hassanein, V. Philipps, C. S. Pitcher, J. Roth, W. R. Wampler, and D. G. Whyte. *Nuclear Fusion*, **41**:1967, 2001.

[20] E. D. Fredrickson, C. Z. Cheng, D. Darrow, G. Fu, N. N. Gorelenkov, G. Kramer, S. S. Medley, J. Menard, and L. Roquemore. *Physics of Plasmas*, **10**:2852, 2003.

[21] O. Mitarai. *Plasma physics and controlled fusion*, **41**:1469, 1999.

[22] O. Mitarai and Y. Takase. *Fusion science and technology*, **43**:67, 2003.

[23] O. Mitarai, R. Yoshino, and K. Ushigusa. *Nuclear fusion*, **42**:1257, 2002.

[24] Y. M. Peng and D.J. Strickler. *Nuclear Fusion*, **26**:769, 1986.

[25] S. M. Motevalli, N. Dashtban, F. Fadaeia, and F. Asadi. *Bulg. J. Phys*, **41**:209, 2014.

[26] S. J. Brereton and M.S. Kazimi. *Fusion Engineering and Design*, **6**:207, 1988.

[27] A. Y. Chirkov and V.I. Khvesyuk. *Fusion Technology*, **39**:406, 2001.

[28] W. R. Fundamenski and A. Harms. *Fusion technology*, **29**:313, 1996.

[29] J. E. Menard, R. E. Bell, E. D. Fredrickson, D. A. Gates, S. M. Kaye, B. P. LeBlanc, R. Maingi, S. S. Medley, W. Park, S. A. Sabbagh, A. Sontag, D. Stutman, K. Tritz, and W. Zhu. *Nuclear Fusion*, **45**:539, 2005.

[30] J. Ongena and G. V. Oost. *Fusion Science and Technology*, **61**:3, 2012.

[31] A. A. Harms, K. F. Schoepf, and D. R. Kingdon. *Principles of fusion energy: an introduction to fusion energy for students of science and engineering*. Science, 1th edition, 2000.

[32] J. P. Freidberg. *Plasma physics and fusion energy*. Cambridge university press, 1th edition, 2008.

[33] X. Z. Li, Q. M. Wei, and B. Liu. *Nuclear Fusion*, **48**:125003, 2008.

[34] H. S. Bosch and G. Hale. *Nuclear fusion*, **32**:611, 1992.

[35] J. R. McNally Jr, K. E. Rothe, and R. D. Sharp. *Fusion reactivity graphs and tables for charged particle reactions*. Oak Ridge National Laboratory, 1th edition, 1979.

[36] S. Motevalli and F. Fadaei. *International Journal of Modern Physics E*, **21**:1250078, 2012.

[37] L. Hively. *Nuclear Fusion*, **17**:873, 1977.

[38] H. Marsuura, Y. Nakao, K. Kudo, O. Mitarai, and M. Ohta. *12th International Conference on Emerging Nuclear Energy Systems 2005, ICENES 2005*, **2**:845, 2005.

[39] B. Trubnikov. *Reviews of Plasma Physics*, **7**:345, 1979.

[40] G. Vlad. *Il Nuovo Cimento B (1971-1996)*, **84**:141, 1984.

[41] O. Mitarai, Y. Takase, A. Ejiri, S. Shiraiwa, H. Kasahara, T. Yamada, S. Ohara, TST-2 Team, K. Nakamura, A. Iyomasa, M. Hasegawa, H. Idei, M. Sakamoto, K. Hanada, and et al. *Journal of plasma and fusion research*, **80**:549, 2004.

[42] M. Ishiguro, K. Hanada, H. Liu, H. Zushi, K. Nakamura, A. Fujisawa, H. Idei, Y. Nagashima, M. Hasegawa, S. Tashima, Y. Takase, Y. Kishimoto, O. Mitarai, S. Kawasaki, H. Nakashima, and A. Higashijima. *Physics of Plasmas*, **19**:062508, 2012.

[43] T. Watanabe, O. Mitarai, and H. Matsuura. *Plasma and Fusion Research*, **10**:3405054, 2015.

[44] O. Mitarai, H. Matsuura, T. Omori, S. Kajimoto, T. Takahashi, S. Koike, and K. Nakamura. *Fusion Engineering and Design*, **136**:82, 2018.

[45] O. Mitarai. *Fusion Engineering and Design*, **26**:605, 1995.

[46] O. Mitarai, A. Hirose, and H.M. Skarsgard. *Fusion Technology*, **20**:208, 1991.